On the Channel Estimation Performance of NOMA Systems: Experimental Implementation of Real-Time Downlink NOMA-OFDM

Joana Angjo, Mehmet Mert Tuncer, Ege Akertek, Hakan Alakoca, Mehmet Başaran, and Lütfiye Durak-Ata
Information and Communications Research Group (ICRG)
Informatics Institute, Istanbul Technical University, Istanbul, Turkey
{angjo16, tuncerm15, akertek15, alakoca, mehmetbasaran, durakata}@itu.edu.tr

***Abstract*—Due to the exponential growth in the number of connected devices, the utilization of available resources becomes challenging. To meet this demand, novel techniques with significantly higher gain for efficient spectrum usage and reduced latency are required. Non-orthogonal multiple access (NOMA) is expected to be a promising solution for the scarcity of spectrum resources, which are shared in a non-orthogonal way such that multiple users can access the same frequency and time slots simultaneously. Although many studies concentrate on NOMA, a few of them give insight into how the channel estimation and channel quantization affect the performance of the system. Related to this issue, this study focuses on a downlink NOMA implementation. In the first part, we mainly concentrate on the analysis of the effect of channel estimation and channel quantization on the bit error rate (BER) performance with MATLAB simulations. For the second part, the BER performance of the system is analyzed through a practical two-user downlink NOMA system implemented with software-defined radios (SDRs).**

***Index Terms*—Non-orthogonal multiple access (NOMA), successive interference cancellation (SIC), bit error rate (BER), channel quantization, channel estimation, orthogonal frequency-division multiplexing (OFDM), software-defined radio (SDR), universal software radio peripheral (USRP).**

I. Introduction

Wireless communication systems have a significant impact on enabling users and devices to reach and share information. However, single-carrier modulation introduces inter-symbol interference and the existing multi-carrier modulation methods do not solve the problem of scarcity of resources [1]. Because of the emergent need for new and effective solutions, a lot of recent studies have been concentrated on non-orthogonal multiple access (NOMA) schemes [2], [3] .

In the literature, power-domain NOMA and code-domain NOMA are the two mainstream types of multi-access techniques [4]. While the former focuses on achieving non-orthogonality in the power domain by assigning different power levels to different users, the latter multiplexes signals by employing spreading sequences with non-orthogonal cross-correlation for distinct users [5].

This study focuses on power-domain NOMA, which is realized by the idea of superposition coding (SC) in the transmitter side and successive interference cancellation (SIC) in the receiver side [6]. According to the state of the respective channel strength, a power level is allocated to each user. The transmitted signal is the superposition of all of the power-allocated signals belonging to the users. On the receiver side, the signals are decoded beginning from the strongest one to the weakest through means of SIC. The decoded signal is considered as interference for the next one to be decoded, thus, there is a subtraction of the previously decoded signal occurring in each step at the receiver [7].

Although the allocated power level of the user closer to the base station is relatively low compared to the power levels of the others, it is proved that this user does not fail to decode the signal with a high level of correctness, which makes SIC a beneficial part for NOMA architecture [8], [9]. Even though the receiver architecture is more complex than the previous generations, this entanglement comes with its benefit; considering that both the energy efficiency and spectrum efficiency are at an optimum level despite the tremendous number of users sharing the same channel [10]. NOMA is adaptable to the previously used technologies as well, thus, incorporating it in future wireless systems does not demand a new and expensive infrastructure [11]. For the channel estimation in orthogonal frequency division multiplexing (OFDM)-based NOMA, the modulated data signals are divided into multiple subcarriers to form the NOMA-OFDM symbols [12]. The number of subcarriers is N, which corresponds to the number of OFDM symbols. Insertion blocks are applied to transmit known data, which assist to the channel estimation at the receiver side [13]. Channel quantization is integrated into NOMA-OFDM based on the studies as given in [14], [15]. Implementation of over-the-air systems can be achieved by utilizing universal software radio peripherals (USRPs) [16], [17]. Software-defined radio (SDR) is a platform that can be used to implement different communication systems with tunable carrier frequencies, flexible signal bandwidths and monitored transmission power [18]-[20]. Although various NOMA schemes and system models have been already investigated, most of them are designed assuming perfect channel state information (P-CSI) condition, thus, they are insufficient in giving a specific analysis on how the performance for both users is affected by channel estimation and quantization. In addition, the current real-time implemen-

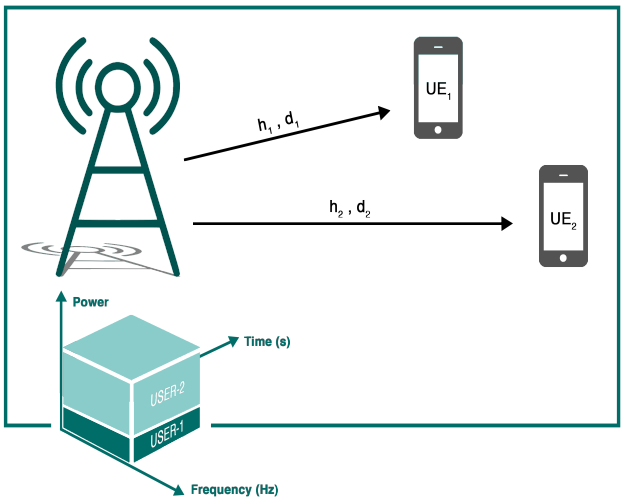

Fig. 1: A power-domain downlink scenario using a single BS and two UEs. Available resources such as frequency, time and code are shared by both UEs.

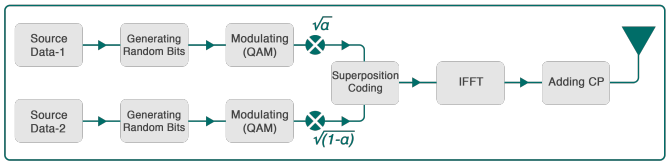

Fig. 2: Block diagram of power-domain NOMA-OFDM based transmitter.

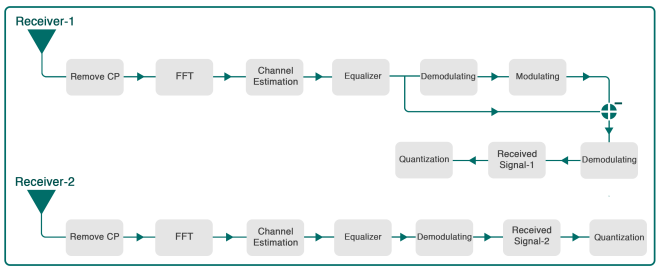

Fig. 3: Block diagram of power-domain NOMA-OFDM based receiver.

tations of NOMA in the literature are currently limited [21], [22]. It is worth to mention that due to its characteristics, this study can be useful for the implementation of NB-IoT technology [23]. Motivated by the aforementioned studies, our main contributions in this study are itemized as below:

- *Channel estimation impacts:* Since in most of the studies related to the downlink NOMA, the channel is perfectly known by the whole users, a downlink NOMA-OFDM based network is investigated considering channel estimation aspect that is measured by the pilot tones.
- *Channel quantization levels:* The effects of channel quantization on the overall bit error rate (BER) performance are addressed and analyzed.
- *Real-time system implementation:* A real-time implementation is performed by using USRPs to realize the system under hardware impairments. A real-time physical-layer link performance is investigated to characterize channel estimation effects on NOMA-OFDM systems.

The remainder of this work is organized as follows. Section II consists of the system model introduction, which describes the power-domain downlink NOMA-OFDM. Section III explains the NOMA-OFDM testbed built upon SDRs. Then, in Section IV the results and observations are discussed. Finally, the paper is concluded in Section V.

II. System Model

A power-domain NOMA based downlink OFDM signal model is considered with a single transmitter and two receiver nodes, as illustrated in Fig. 1. Transmitter node is represented as the base station (BS), two receiver nodes are given as user equipment (UE) UE-1 and UE-2, respectively. Two different random signals are generated and power is allocated at the BS to UEs before the transmission, considering the procedure of the signal demodulation at the receiver side.

Let $X_{1,l}$ and $X_{2,l}$ denote the modulated signals at the BS corresponding to UE-1 and UE-2, respectively. Here, l denotes the l-th modulated symbol. SC signals are transmitted by the BS so as to distribute available resources to UEs. At the transmitter side, SC signals are given as $s_1 = \sqrt{\alpha}X_{1,l}$ and $s_2 = \sqrt{1-\alpha}X_{2,l}$ for UE-1 and UE-2, respectively, where α represents the power allocation factor for power-domain NOMA. A NOMA-OFDM based signal model is considered in order to have precise channel tracking and estimation instead of generic NOMA. Number of subcarriers are given as N with subcarrier distribution of comb type pilot subcarriers starting at every P subcarriers, where $\mathcal{P}$ represents the pilot subcarrier set. Pilot subcarriers are generated independently and used in the channel estimation process for each UE. After subcarrier allocation, time domain signals at the BS can be defined as

$$x_{k,n} = \frac{1}{N}\sum_{l=0}^{N-1}(\sqrt{\alpha}X_{1,l} + \sqrt{1-\alpha}X_{2,l})e^{\frac{j2\pi kn}{N}}, \qquad (1)$$

where $k = \{1, 2\}$ denotes the index of UEs. Then, last L subcarriers are copied at the beginning of the NOMA-OFDM symbols as cyclic prefix (CP) insertion. The transmitter block diagram is illustrated in Fig. 2, while the receiver block diagram of NOMA-OFDM is illustrated in Fig. 3. For each UE, the received time-domain signals can be given as

$$y_{k,n} = \sqrt{\frac{P_t}{d_k^v}}x_{k,n} * h_{k,n} + w_{k,n}, \qquad (2)$$

where P_t, d_k, and v represent transmitted power at the BS, the distance between BS and UEs, and path loss coefficient, respectively, and * denotes the convolution operation. Also, $h_{k,n}$ is given as Rayleigh fading channel coefficient. We also note that corresponding channel coefficients for UE-1 and UE-2 are given as $h_{1,n}$ and $h_{2,n}$, respectively, with $h_{1,n} > h_{2,n}$, since

$d_1 < d_2$. Furthermore, $w_{k,n}$ stands for AWGN component for each RF receiver with zero mean and σ^2 variance.

At the receiver side, received RF signals are processed through CP removal and FFT operations for each UE. In order to detect individual symbols, channel estimation processes are handled first via pilot subcarriers, where $\epsilon_{k,l}$ represents the channel estimation error. Before detecting the transmitted symbols, an equalizer is used to compensate the destructive effects of the channel. The channel estimates are denoted by $\widehat{H}_{k,l}$. When $l \in \mathcal{P}$ and for each UE for $k = \{1, 2\}$, we obtain corrupted channel estimates in frequency domain as

$$\begin{aligned}\widehat{H}_{k,l} &= \frac{Y_{k,l}}{X_{k,l}} = \frac{X_{k,l}H_{k,l} + W_{k,l}}{X_{k,l}} = H_{k,l} + \frac{W_{k,l}}{X_{k,l}} \\ &= H_{k,l} + \epsilon_{k,l}, \end{aligned} \tag{3}$$

where $Y_{k,l}$, $H_{k,l}$ and $\epsilon_{k,l}$ denote the received signal, channel impulse response, and channel estimation error, respectively. The channel estimation process using pilot subcarriers via linear interpolation can be expressed as

$$\widehat{H}_{q_k,l} = \frac{\widehat{H}_{k,lP}(X_{k,(l+1)P} - X_{q_k,l}) + \widehat{H}_{k,(l+1)P}(X_{q_k,l} - X_{k,lP})}{X_{k,(l+1)P} - X_{k,lP}}, \tag{4}$$

where $q_k = \{lP+1, \ldots, (l+1)P-1\}$. The received information symbols for each UE can be expressed using minimum mean square error (MMSE) estimation as

$$\widehat{X}_{k,l} = \frac{Y_{k,l}}{\widehat{H}_{k,l}} = \frac{X_{k,l}H_{k,l}}{H_{k,l} + \epsilon_{k,l}} + \frac{W_{k,l}}{H_{k,l} + \epsilon_{k,l}}, \tag{5}$$

for $l \in \mathcal{N} \setminus \mathcal{P}$, where $\mathcal{N}$ represents the total subcarrier set. For the near user UE-1, which operates SIC at the receiver side, the estimated signal is given as $\widehat{X}_{1,l}$. Considering estimated signals for the far user, $\widehat{X}_{2,l}$, SIC process is no longer needed since the high-powered signal can be directly demodulated, by assuming the other signal directly as noise. $\widehat{X}_{1,l}$ and $\widehat{X}_{2,l}$ can be expressed as

$$\widehat{X}_{1,l} = \frac{Y_{1,l} - \sqrt{1-\alpha}\widehat{X}_{2,l}\widehat{H}_{2,l}}{\sqrt{\alpha}\widehat{H}_{1,l}}, \tag{6}$$

$$\widehat{X}_{2,l} = \frac{Y_{2,l}}{\sqrt{1-\alpha}\widehat{H}_{2,l}}. \tag{7}$$

Estimated signals are demodulated and converted into bits so as to evaluate BER performance. Furthermore, channel quantization has significant impacts on transmitted and received signals due to analog-to-digital and digital-to-analog converter components. We also note that Lloyd-Max scalar channel quantizer is applied after the channel estimation process in order to monitor the channel quantization effect [24].

III. Testbed Environment

A real-time downlink NOMA-OFDM based network is realized with a single BS and two UEs employing software-defined radios (SDRs). Real-time measurements are operated at Information and Communications Research Group (ICRG) Laboratory, Istanbul Technical University, where testbed environment is given in Fig. 4. Testbed environment consists

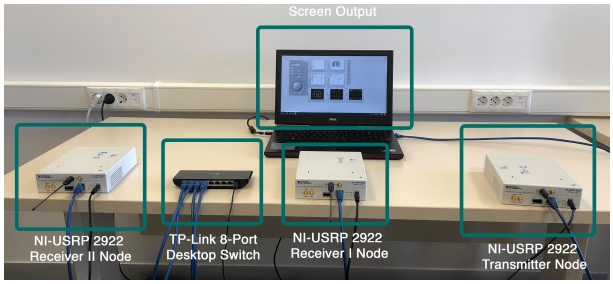

Fig. 4: Testbed environment at Istanbul Technical University ICRG Laboratory for NOMA-OFDM system.

TABLE I: Parameters for the NOMA-OFDM testbed

Parameters	**Selected values**
Carrier Frequency	890 MHz
I/Q Rate	500 kS/sec
Bandwidth	0.5 MHz
Modulation	4-QAM
Power Allocation Factor	α = 0.2
Transmitter Gain	8 dB
Distance of Receiver 1 from Transmitter	1 m
Distance of Receiver 2 from Transmitter	2 m
Receiver Gain	0-8 dB
Zero Padding Length	75 subcarriers
IFFT Length	256 subcarriers
η	1/6, 1/10, 1/18, 1/30
CP Length	64 samples

of three USRP 2922 nodes as BS and UEs, which can be operated between 400 MHz and 4.4 GHz frequency band, a GigE switch and a PC, as the signal processing unit. The host computer runs LabVIEW, the visual programming language that performs the signal processing following with the NOMA-OFDM system. The hardware components, which are the transmitter and the receivers are connected to VERT400 antennas. They are connected to an 8-port gigabit desktop switch through Ethernet cables. Simulation parameters that are used during the realization of the system are referred to as Table I.

The transmitted bits are processed in order to be applied to the RF requirements. Converted to an analog wave with 16 bit quantization precision, the signal is up-converted to 890 MHz frequency and it is transmitted from the TX antenna to the RX antenna. The opposite process takes place at the receiver part with 14-bit quantization precision [25].

Software components consist of two main parts: hardware drivers and signal processing blocks. Hardware drivers are principally adequate to control SDR nodes. They are also responsible for adopting central frequency, bandwidth and antenna mode.

Signal processing blocks are used for both signal generation and signal reception operations. On the signal generation side, a pre-determined frame structure is used to control channel estimation performance. According to the OFDM frame architecture, 38-subcarriers are used as zero padding in the beginning of the frame to reduce hardware specific impacts such as clipping. In a similar way, 37 subcarriers are also used as zero padding at the end of the frame. We also reserve a single subcarrier for

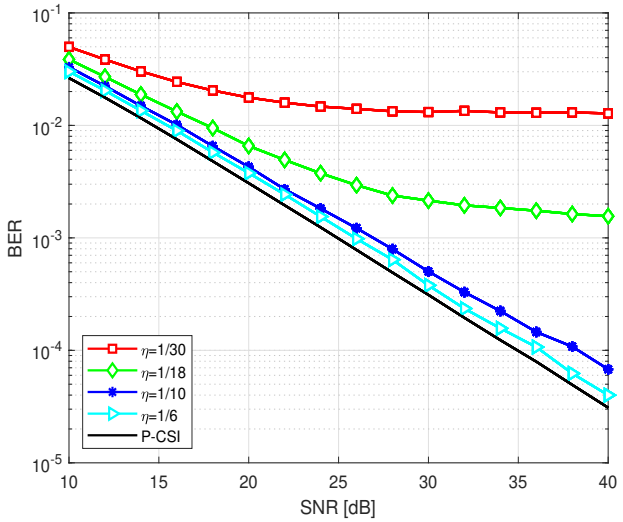

Fig. 5: Channel estimation impact on BER performance with varied η ratios on UE-1.

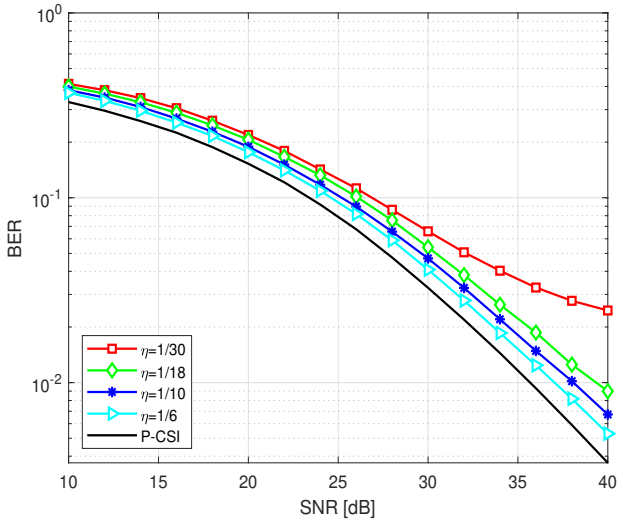

Fig. 6: Channel estimation impact on BER performance with varied η ratios on UE-2.

the DC-component. Payload data is sliced into two equal parts before and after the DC component as 180 subcarriers in total. In order to achieve channel estimation, pilot tones are used and utilized by considering pilot-to payload data ratio. Furthermore, payload data and pilot tones are generated via 4-QAM symbols. Both UE-1 and UE-2 payload data symbols are generated by different pseudo-noise dependent bits. We also noted that in order to reduce the delay spread of the channel, CP length is selected as 64 samples.

For simplicity, RF gain of the transmitter USRP is fixed as 8 dB. The receiver gain is selected from 0 dB to 8 dB with a 2 dB step. The experiments are conducted for four different η values, which represent the ratio of used pilot tones to N. For specific η and receiver gain values, the transmitter sends data to the receiver fifteen times for a period of 60 seconds each. The average BER value is computed from the observed information accordingly.

IV. Simulations and Testbed Results

In this section, several scenarios are considered and corresponding simulations are performed. Moreover, the results from the testbed are analyzed. The following simulations are handled for OFDM based NOMA. N is selected as 180 subcarriers, L is determined as 64 samples. Also, 4-QAM modulated signals are generated at the BS for both UE-1 and UE-2. Distances between BS and each UE, d_1 and d_2, are selected as 1m and 2m, respectively. Simulations are performed under Rayleigh fading channel with a path loss coefficient $v = 3.4$.

A. Impact of Channel Estimation on BER Performance

In order to operate channel tracking in NOMA-OFDM, downlink pilot subcarriers are used through the MMSE estimator. When η value increases, the results become closer to the P-CSI case. In the simulations, α is selected as 0.2. Fig. 5 shows the impact of channel estimation on BER performance under varied η ratios for UE-1. Increasing η leads to a decrease of BER, as expected. For instance, under 30 dB signal-to-noise-ratio (SNR), η = $\{1/6, 1/10, 1/18, 1/30\}$ are performed, providing BER levels as $\{1.31\times10^{-2}, 2.14\times10^{-3}, 5.02\times10^{-4}, 3.78 \times 10^{-4}\}$, respectively. Also, BER performance of the far UE is given under varied η ratios in Fig. 6. BER performance of UE-1 is better than UE-2 due to the path loss effect. In addition, the channel estimation impact follows the same trend to UE-2 considering varied η. For example, under 36 dB SNR, η = $\{1/6, 1/10, 1/18, 1/30\}$ are performed, providing BER levels $\{3.27 \times 10^{-2}, 1.87 \times 10^{-2}, 1.48 \times 10^{-2}, 1.24 \times 10^{-2}\}$, respectively.

B. Impact of Channel Quantization on BER Performance

Fig. 7 shows the constellation diagram of the received complex signals in both UE-1 and UE-2. The diagram looks like 16-QAM constellation diagram because of the superposition of two 4-QAM signals. Fig. 8 shows the constellation diagram of the received UE1 signal after SIC is performed. This constellation diagram looks like 16-QAM as well, however, the demodulation is performed only based on which quadrant each received bit belongs to, that is why UE-1 still demodulates the signal with overall good performance. From Fig. 7 and Fig. 8 it is also shown that real-time implementation of two user's NOMA-OFDM based network is perfectly operated with pilot tones.

Fig. 9 depicts channel quantization impact on NOMA-OFDM based system for UE-1 and UE-2 under $\eta = 1/10$ and $\eta = 1/18$. Through the analyses, both channel estimation and channel quantization impact can be observed. There are three quantization levels for digitized estimated channels that are considered: 4-bits, 6-bits and 8-bits quantization with 10^5 sampling rate using Lloyd-Max channel quantizer. When using 4-bit quantization, then 2^4 quantization levels are achieved. BER performances under $\eta = 1/10$ and $\eta = 1/18$ for UE-1 are presented in Fig. 9 (a) and Fig. 9 (b), respectively. Increasing

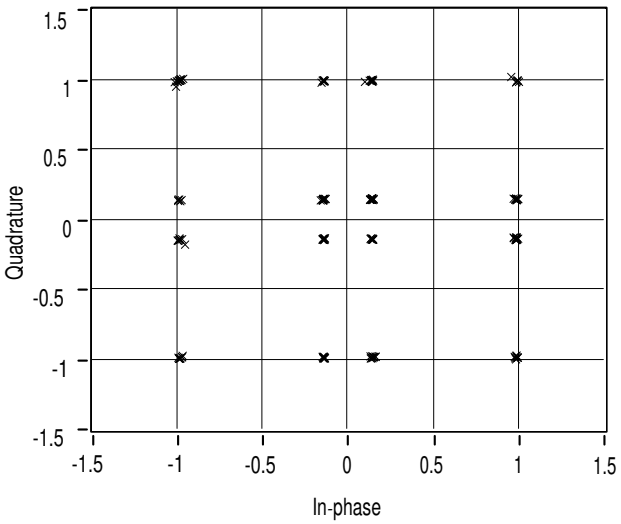

Fig. 7: A snapshot of real-time constellation diagram of collected signals of UE-1 and UE-2 at the receiver.

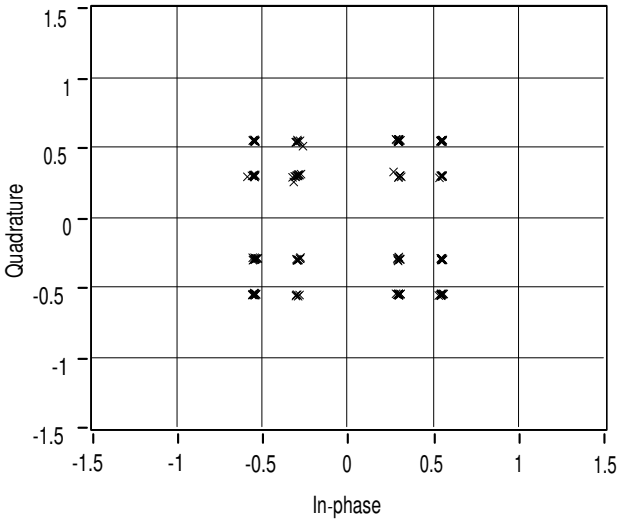

Fig. 8: A snapshot of constellation diagram of UE-1 after SIC operation at the receiver.

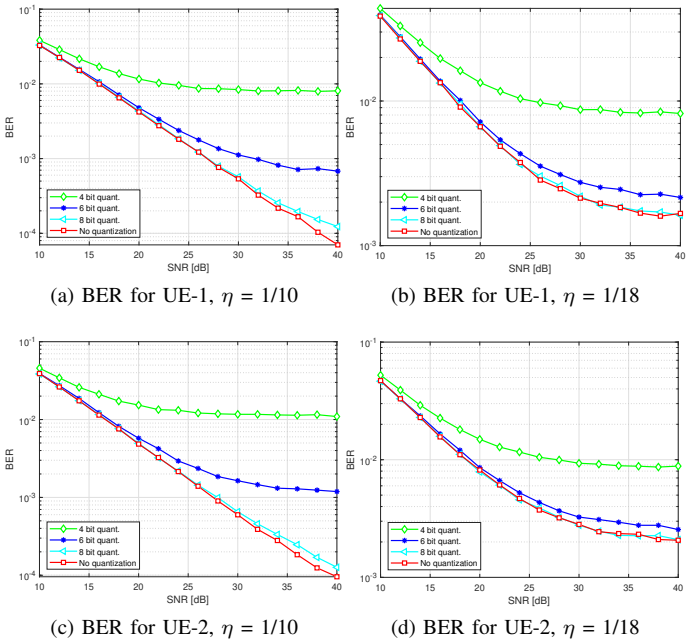

(a) BER for UE-1, η = 1/10 (b) BER for UE-1, η = 1/18

(c) BER for UE-2, η = 1/10 (d) BER for UE-2, η = 1/18

Fig. 9: BER simulations with varying channel quantization.

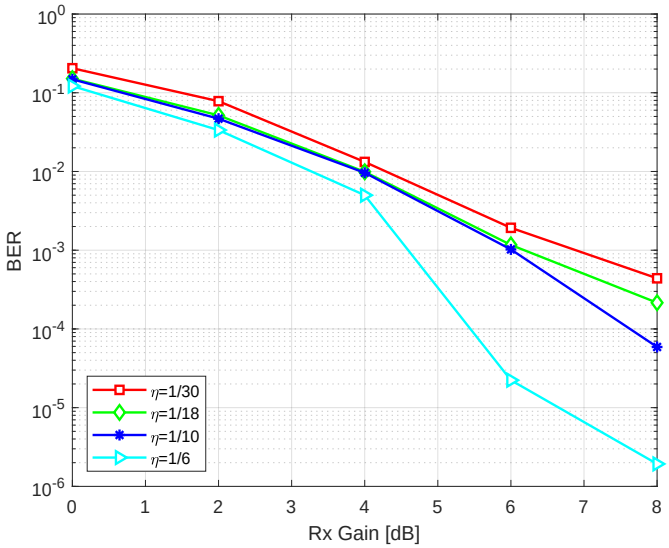

Fig. 10: Channel estimation impact on BER in testbed implementation with varied η ratios on UE-1.

the number of quantization bits can help to approach to the case in which only channel estimation is performed. Thus, the BER values corresponding to the latter case are close to the 8 bit quantization case, as expected. UE-2 case is shown in 9 (c) and 9 (d). As can be observed, performance degradation occurs when $\eta = 1/18$ for both UE-1 and UE-2, since the demodulation is performed upon less information regarding the channel.

C. Impact of Channel Estimation on Practical NOMA-OFDM Testbed

Fig. 10 and Fig. 11 illustrate the average BER achieved during the experiment for a fixed value of 8 dB transmitter gain, while the receiver gain is being altered. Simultaneously, channel estimation is performed with different η values $1/6$, $1/10$, $1/18$, and $1/30$, accordingly. As seen from the figures, the overall performance of the closer user is better compared to that of the far user. First user's lowest BER is achieved for the maximum number of pilot usage and the highest gain value is 1.93×10^{-6}, while the user's second lowest BER achieved for the same conditions is 7.96×10^{-5}. Finally, increasing the gain of receivers also significantly improves the performance of the system, as expected.

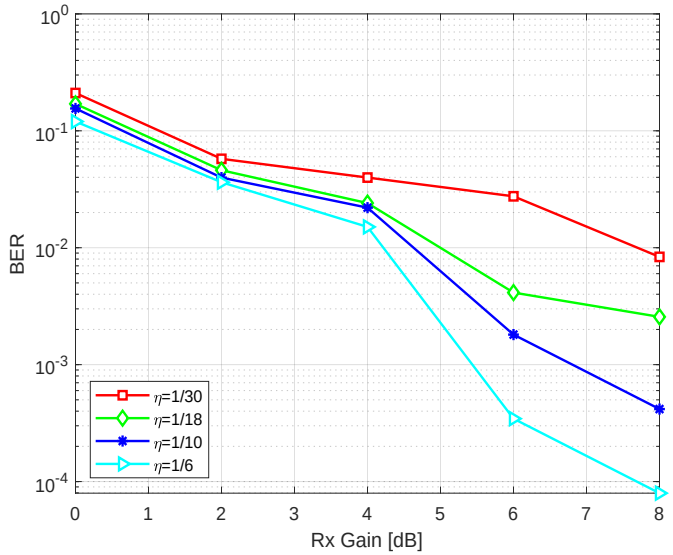

Fig. 11: Channel estimation impact on BER in testbed implementation with varied η ratios on UE-2.

In order to check the accuracy of our study, we compare the results of simulations and testbed measurements regarding the BER performance. For the simulations, we obtain graphs showing how BER is affected by SNR and for the testbed, we check how link-quality impacts BER. As seen from the graphs, for the 5 dB receiver gain the obtained results from simulations and testbed measurements follow the same track. The more the gain is increased, the lower the BER values are obtained.

V. Conclusion

In this paper, a power-domain downlink NOMA-OFDM performance is investigated under imperfect channel conditions considering SC and SIC. According to the simulation results, underestimation of the channel causes performance degradation. However, pilot insertion should be decided carefully due to the overhead caused by the pilot tones. Also, channel quantization impact is covered with channel estimation effect via the Lloyd-Max algorithm and BER simulations are provided. Increasing the quantization level improves the result, but at the same time, this increases the computational complexity of the system. In addition to these, BER results are obtained from a practical downlink NOMA system based on a SDR platform with different receiver gain values and pilot-to-data ratios.

Acknowledgment

This work is supported in part by Istanbul Technical University (ITU) Vodafone Future Lab under Project No. ITUVF20191001P07.

References

[1] B. Chethan, B. N. Ravisimha, and M. Kurian, "The effects of inter symbol interference (ISI) and FIR pulse shaping filters: a survey," *Int. J. of Advanced Res. Elect. Electron. and Instrumentation Eng.* vol. 3, no. 5, 9411-9416, 2014.

[2] Y. Liu, Z. Qin, M. Elkashlan, Z. Ding, A. Nallanathan, and L. Hanzo, "Nonorthogonal Multiple Access for 5G and Beyond," *Proceedings of the IEEE*, vol. 105, no. 12, pp. 2347-2381, 2017.

[3] L. Song, Y. Li, Z. Ding, and H. V. Poor, "Resource Management in Non-Orthogonal Multiple Access Networks for 5G and Beyond," *IEEE Network*, vol. 31, no. 4, pp. 8-14, 2017.

[4] M. Aldababsa, M. Toka, S. Gökçeli, G. K. Kurt, and O. Kucur, "A tutorial on nonorthogonal multiple access for 5G and beyond," *Wireless Commun. and Mobile Comput.,*, 2018.

[5] S. R. Islam, M. Zeng, O. A. Dobre, and K. S. Kwak, "Nonorthogonal Multiple Access (NOMA): How It Meets 5G and Beyond." *Wiley 5G Ref: The Essential 5G Reference Online*, 1-28, 2019.

[6] C. Yan, A. Harada, A. Benjebbour, Y. Lan, A. Li, and H. Jiang, "Receiver Design for Downlink Non-Orthogonal Multiple Access (NOMA)," *IEEE 81st Vehicular Technology Conference (VTC Spring)*, pp. 1-6, 2015.

[7] A. Benjebbour, K. Saito, A. Li, Y. Kishiyama, and T. Nakamura, "Non-orthogonal multiple access (NOMA): Concept, performance evaluation and experimental trials," *Conf. Wireless Networks and Mobile Commun. (WINCOM)*. pp. 1-6, 2015.

[8] K. Higuchi and A. Benjebbour, "Non-orthogonal multiple access (NOMA) with successive interference cancellation for future radio access," *IEICE Trans. Commun.*, vol. 98, no. 3, pp. 403–414, 2015.

[9] R. Razavi, M. Dianati, and M. Imran, "Non-Orthogonal Multiple Access for future radio access", *5G Mobile Communications*, pp. 135-163, 2017.

[10] S. M. Riazul Islam, Ming Zeng, and Octavia A. Dobre. "NOMA in 5G Systems: Exciting Possibilities for Enhancing Spectral Efficiency," *IEEE 5G Tech Focus*, vol. 1, no. 2, June 2017

[11] Z. Ding, X. Lei, G. K. Karagiannidis, R. Schober, J. Yuan, and V. K. Bhargava, "A survey on non-orthogonal multiple access for 5G networks: Research challenges and future trends." *IEEE J. Sel. Areas in Commun.* vol. 35, no. 10, pp. 2181-2195, 2017.

[12] H. Sadia, M. Zeeshan, and S. A. Sheikh, "Performance analysis of downlink power domain NOMA under fading channels," *2018 ELEKTRO*, Mikulov, pp. 1-6, 2018.

[13] P. Sure and C. M. Bhuma, "A survey on OFDM channel estimation techniques based on denoising strategies,"*Eng. Sci. and Technol.* vol. 20, no. 2, pp. 629-636, 2017.

[14] M. Trivellato, F. Boccardi, and H. Huang, "On transceiver design and channel quantization for downlink multiuser MIMO systems with limited feedback," *IEEE J. Sel. Areas in Commun.* vol. 26, no. 8, pp. 1494-1504, 2008.

[15] T. Yoo, N. Jindal, and A. Goldsmith, "Multi-antenna downlink channels with limited feedback and user selection," *IEEE J. Sel. Areas Commun.* vol. 25, no. 7, pp. 1478-1491, 2007.

[16] M. A. Durmaz, C. Göztepe, G. K. Kurt, M. Toka, and O. Kucur, "Non-Orthogonal Multiple Access System Implementation in Software Defined Radios," *27th Signal Process. and Commun. App. Con.*, Sivas, Turkey, pp. 1-4, 2019.

[17] X. Wei et al., "Software Defined Radio Implementation of a Non-Orthogonal Multiple Access System Towards 5G," IEEE Access, vol. 4, pp. 9604-9613, 2016.

[18] L. Dai, B. Wang, Z. Ding, Z. Wang, S. Chen, and L. Hanzo, "A Survey of Non-Orthogonal Multiple Access for 5G," *IEEE Commun. Surveys and Tuts.* vol. 20, no. 3, pp. 2294-2323, Third quarter 2018.

[19] X. Xiong, W. Xiang, K. Zheng, H. Shen, and X. Wei, "An open source SDR-based NOMA system for 5G networks," *IEEE Wireless Commun.* vol. 22, no. 6, pp. 24-32, 2015.

[20] L. Hosni, A. Farid, A. Elsaadany, and M. Safwat, "5G New Radio Prototype Implementation Based on SDR," *Communications and Network*, 12, pp. 1-27, 2020.

[21] E. Khorov, A. Kureev, and I. Levitsky, "NOMA testbed on Wi-Fi," *IEEE 29th Annual International Symposium on Personal, Indoor and Mobile Radio Communications*. pp. 1153-1154, 2018.

[22] X. Wei, Z. Geng, H. Liu, K. Zheng, and R. Xu, "A portable SDR non-orthogonal multiple access testbed for 5g networks," *IEEE 85th Vehicular Technology Conference*. pp. 1-5, 2017

[23] C. B. Mwakwata, H. Malik, M. Mahtab Alam, Y. Le Moullec, S. Parand, and S. Mumtaz, "Narrowband Internet of Things (NB-IoT): From Physical (PHY) and Media Access Control (MAC) Layers Perspectives," *Sensors*, 19(11), 2613, 2019

[24] Y. Samayoa and J. Ostermann, "A Lloyd-Max based quantizer of L-values for AWGN and Rayleigh fading channel," *Sixth Int. Conf. on Wireless Commun. and Signal Process.,* pp. 1-6, 2014

[25] *National Instruments, revised*, USRP, N. 2922 Specifications. 17, 2017.